International Journal of Advances in Engineering and Management (IJAEM)
Volume 4, Issue 12 Dec. 2022, pp: 778-790 www.ijaem.net ISSN: 2395-5252

Passive Control MHD heat and mass transfer over a vertical plate with Viscous Dissipation and convective surface boundary condition

Akindele M. Okedoye[1,2] and Sikiru Yemi Onifade[3]
[1]*Department of Mathematics, Covenant University, Ota, Ogun State, Nigeria*
[2]*Department of Mathematics, Federal University of Petroleum Resources, Effurun, Nigeria*
[3]*Department of Physics, Federal University of Petroleum Resources, Effurun, Nigeria*

Submitted: 18-12-2022 Accepted: 28-12-2022

ABSTRACT: Lubrication, viscometry, and extrusion all involve the flow of liquids, therefore viscous heating is a significant issue. The proportion of heat generated by viscous dissipation to heat carried by molecular conduction is known as the Brinkman number, and it has no dimensions. i.e., the proportion of viscous heating to outside heating. The contribution of passive control MHD heat and mass transfer over a vertical plate with Viscous dissipation and convective surface boundary condition is crucial in the area of engineering and designs. The nonlinear partial differential equations governing the flow was modelled to include buoyancy, Lorentz force, reactivity parameter and velocity slip factor. We transformed the equations to an ordinary system of equations using appropriate self-similar variables. The resulting ordinary differential equations are solve using Homotopy Analysis implemented by Wolfram Mathematical software Mathematical 12.2. The results are presented in Tables and graphs and well discussed. From the results obtained, it was discovered that increase in stretching velocity, and thermal buoyancy respectively are seen to increase velocity distributions. Effect of other parameters as well as wall rate transfer well-presented and discussed.

KEYWORDS: Magnetohydrodynamic, Viscous dissipation, Flow Parameters, Skin-friction Parameters, Boundary Condition, Vertical plate, Convective surface. Heat and Mass transfer.
MSC SUBJECT CLASSIFICATION:76A05, 76B75, 76D05

I. INTRODUCTION

The Navier-Stokes model of fluid dynamics and the Maxwell's equations of electromagnetism both produce forces on fluid as a result of the effects of magnetic field-induced current [1]. The aerospace industry, chemical and petrochemical engineering, heat exchangers, nuclear reactors, and combustion systems are just a few examples of the sciences and engineering fields where MHD in relation to nanofluid has a wide range of applications in enhancing thermal conductivity and heat transfer. The effect of temperature and nanoparticle size on the viscosity of nanofluids at a variety of temperatures is mostly due to large concentrations of nanoparticles [2,3]. Given this, it is necessary to estimate the precise function of nanoparticles in enhancing heat transfer by taking into account the influence of nanofluid characteristics on temperature and volume fraction of nanoparticles. The discussion of the consequences of viscosity and thermal conductivity of Al2O3-water nanofluid was sparked by this [4]. When the buoyancy parameter is increased, the fluid velocity increases and the thermal boundary layer decreases, according to the Homotopy analysis approach used to study the effect of buoyancy and thermal MHD flow across a stretching porous sheet [5]. Due to its dynamic interaction with a magnetic field, magnetic induction is the generation of an electromotive force or voltage across an electrical conductor [6]. Hannes Alfven was the one who first proposed the MHD idea, which was recognized in 1970. In contrast to previous studies, the effects of Brownian motion and thermophoresis on the

International Journal of Advances in Engineering and Management (IJAEM)
Volume 4, Issue 12 Dec. 2022, pp: 778-790 www.ijaem.net ISSN: 2395-5252

volume fraction of nanoparticles are actively handled on the boundary [7]. The active control model can be used to regulate both the rate of mass transfer at the wall and the thickness of the boundary layer. Over the years, a number of authors in the fields of science, engineering, and many sectors have been interested in the flow of nanofluid through a porous medium [8]. The length of the runway, approach speed, climb rate, cargo capacity, operating range, and noise and emission levels in the neighborhood are all significantly influenced by the performance of airplane wings. Wing performance is frequently diminished by flow separation, which is frequently a result of the airfoil profile's aerodynamic design. The notion of active control systems, which is based on real-time processing and allows them to react to excitation utilizing sensors embedded into the device, is said to be more sophisticated than passive control systems.

The interplay of thermal radiation and unsteady MHD flow past a vertical porous plate was investigated in the study of Samad & Mansur-Rahman [9]. A permeable material was used to submerge the plate. While Md. Anwar Hossain & Munir [10] provided analysis of a 2-D mixed convection flow of viscous incompressible temperature dependent viscous fluid past a vertical plate, Makinde & Sibanda [5] focused on MHD mixed convective flow and heat transfer past a vertical plate dipped in a porous medium with constant wall suction. Mahmoud [12] demonstrated how altering viscosity impacts hydromagnetic boundary layer flow along a constantly moving vertical plate sensitive to radiation, while Fang [11] examined how fluid property variation affects boundary layers of a stretching surface. According to the research of M. Anwar Hossain et al. [13], radiation has an impact on the free convection flow of a fluid with changing viscosity on a porous vertical plate. Poornima & Reddy [14] established sustained free convective boundary layer flow of a radiating nanofluid in the presence of a transverse magnetic field using a non-linear stretching sheet. The effects of thermal stratification brought on by solar radiation, Brownian motion, and thermophoresis on the MHD boundary layer flow of nanofluid were examined by Kandasamy et al. [15]. In the presence of thermal radiation and viscous dissipation, Motsumi & Makinde's [16] numerical investigation of the boundary layer flow of a nanofluid across a permeable moving flat plate. Plane Poiseuille flow with asymmetric convective heat transfer was taken into account in the study of Makinde and Aziz [18].

Despite the contributions of the above authours and numerous other authours, there is still need to understand the contribution of Passive Control MHD heat and mass transfer over a vertical plate with Viscous Dissipation and convective surface boundary condition is crucial in the area of engineering and designs. Hence this report revisits the work of Aziz et.al [34] and Makinde [33] to include buoyancy, Lorentz force, reactivity parameter and velocity slip factor

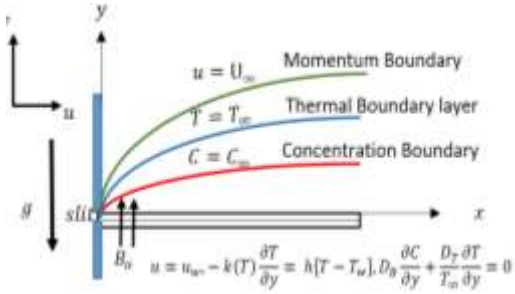

Figure 1. Flow configuration and coordinate system

II PROBLEM FORMULATION

Consider a mixed convection flow over a vertical plate with a steady, laminar hydromagnetic linked heat and mass transfer. The fluid is taken to be Newtonian, electrically conducting, and its temperature and chemical species concentration-related changes in properties are restricted to changes in fluid density. Additionally, there is no applied electric field and no consideration is given to any of the Hall effects or Joule heating (Figure 1).

We presume that the induced magnetic field is insignificant because the majority of industrial fluids have relatively low magnetic Reynolds numbers. The y-axis is normal to the plate's direction, and the x-axis is taken in that direction. The governing equations for this issue can be expressed using the Boussinesq and boundary-layer approximations if u, v, T, and C are the fluid's respective $x-, y-$, temperature, and concentration components.

$$\frac{\partial u}{\partial x}+\frac{\partial v}{\partial y}=0, \qquad (1)$$

$$\rho_f\left(u\frac{\partial u}{\partial x}+v\frac{\partial u}{\partial y}\right)=-\frac{dp}{dx}+\frac{\partial}{\partial y}\left(\mu_T\frac{\partial u}{\partial y}\right) -\sigma(x)\beta_0^2 u+g\beta_t(x)(T-T_\infty) +g\beta_c(x)(C-C_\infty), \qquad (2)$$

$$\rho_f c_p\left(u\frac{\partial T}{\partial x}+v\frac{\partial T}{\partial y}\right)=\frac{\partial}{\partial y}\left(k_T\frac{\partial T}{\partial y}\right) +Q(T-T_\infty)+\mu_f\left(\frac{\partial u}{\partial y}\right)^2, \qquad (3)$$

International Journal of Advances in Engineering and Management (IJAEM)
Volume 4, Issue 12 Dec. 2022, pp: 778-790 www.ijaem.net ISSN: 2395-5252

$$\rho\left(u\frac{\partial C}{\partial x}+v\frac{\partial C}{\partial y}\right)=D\frac{\partial^2 C}{\partial y^2}+\kappa r^2(C-C_\infty). \quad (4)$$

MHD Boundary Layer Flow Past a Moving Plate with Mass Transfer and Binary Chemical Reaction was investigated by [23] and [24]. While internal friction between the surface and fluid particle must be taken into account when calculating thermal conductivity and viscosity dependent on temperature, it is appropriate to assume the mathematical formulation of these dependents as investigated in [25] and [26]. Assuming the same viscosity and thermal conductivity as Wahab et al. [27, 28] formulation, we can state the following:

$$\begin{aligned}\mu_T &= \mu_f\left(1+b_1(T_\infty-T)\right)\\ k_T &= k_f\left(1+b_2(T-T_\infty)\right),\end{aligned} \quad (5)$$

ρ_f is the density of base fluid, $\upsilon_f=\mu_f/\rho_f$is kinematic viscosity of the Nano-fluid.

We write the boundary conditions at the plate surface and deep into the cold fluid as

$$\left.\begin{aligned}u=L_1\left(\frac{\partial u}{\partial y}\right),-k(T)\frac{\partial T}{\partial y}=h[TT_w-T],\\ v=v_w,D_B\frac{\partial C}{\partial y}+\frac{D_T}{T_\infty}\frac{\partial T}{\partial y}=0,\\ u\to U_\infty,T\to T_\infty,C\to C_\infty,\quad \text{as } y\to\infty,\end{aligned}\right\} \quad (6)$$

In equations (6) $L_1=L(Re_x)^{1/2}$ is the velocity slip factor, and L is the initial value of velocity slip factor. The $Re_x=U_\infty x/\nu$ is the local Reynolds number.$u_\infty(x)=ax$ is the velocity of the flow outside the boundary layer, $u_w(x)=cx$ is the velocity of the stretching sheet with c and a being the positive constants determining the strength of the stagnation point and stretching rate.

It is important to note that the normal flow of the fluid at the boundary is assumed to be zero similar to [28]-[30] and that the thermosphoresis is taken into account in the final section of the boundary condition (6). The main goal of this condition is to passively control the volume percentage of nanoparticles at the boundary. This circumstance differs from past studies and offers a more practical perspective.

As $y\to\infty, u\to U_\infty$, $T\to T_\infty$, $C\to C_\infty$ equation (2) becomes

$$a^2x+\frac{\sigma(x)\beta_0^2}{\rho}ax=-\frac{1}{\rho}\frac{dp}{dx} \quad (7)$$

Equation (2) and (3) alongside equation (5) and (7) becomes

$$\begin{aligned}u\frac{\partial u}{\partial x}+v\frac{\partial u}{\partial y}&=U_\infty\frac{\partial U_\infty}{\partial x}-\frac{\sigma(x)\beta_0^2}{\rho}(u-U_\infty)\\ &+\frac{\partial}{\partial y}\left(\mu_f\left(1+b_1(T_\infty-T)\right)\frac{\partial u}{\partial y}\right)\\ &+\frac{g\beta_t(x)}{\rho}(T-T_\infty)+\frac{g\beta_c(x)}{\rho}(C-C_\infty),\end{aligned} \quad (8)$$

$$\begin{aligned}\rho c_p\left(u\frac{\partial T}{\partial x}+v\frac{\partial T}{\partial y}\right)&=+Q(T-T_\infty)+\mu(T)\left(\frac{\partial u}{\partial y}\right)^2\\ &\frac{\partial}{\partial y}\left(k_f\left(1+b_2(T-T_\infty)\right)\frac{\partial T}{\partial y}\right)\end{aligned} \quad (9)$$

III SIMILARITY TRANSFORMATION

Equations (1), (4), (8), and (9) can be transformed by defining an independent variable as being equal to η and a dependent variable fin terms of the stream function ψ as

$$\eta=y\sqrt{\frac{U_w}{\nu x}},\psi=\sqrt{\nu x U_w}f(\eta) \quad (10)$$

The dimensionless values for temperature and concentration are

$$\theta(\eta)=\frac{T-T_\infty}{T_w-T_\infty},\phi(\eta)=\frac{C-C_\infty}{C_w-C_\infty}. \quad (11)$$

The translated horizontal and axial velocities from Equation (11) are as follows;

$$u=cxf'(\eta),v=-\sqrt{c\nu}f(\eta)\text{with }\eta=y\sqrt{\frac{c}{\nu}} \quad (12)$$

Equation (1) is satisfied exactly by equation (12), and equations (8), (9) and (4) are translated to the dimensionless velocity, temperature, and concentration, respectively, as shown in the following.

$$\begin{aligned}\frac{\partial}{\partial\eta}\left(\left(1-\beta\theta(\eta)\right)\frac{\partial^2 f(\eta)}{\partial\eta^2}\right)+\frac{1}{2}f(\eta)\frac{\partial^2 f(\eta)}{\partial\eta^2}\\ +Ha\left(1-\frac{\partial f(\eta)}{\partial\eta}\right)+Grt\theta(\eta)\\ +Grc\phi(\eta)+A^2=0,\end{aligned} \quad (13)$$

$$\begin{aligned}\frac{\partial}{\partial\eta}\left(\left(1+\beta\theta(\eta)\right)\frac{\partial\theta(\eta)}{\partial\eta}\right)+\frac{1}{2}Prf(\eta)\frac{\partial\theta(\eta)}{\partial\eta}\\ +Pr\delta\theta(\eta)+PrEc\left(\frac{\partial^2 f(\eta)}{\partial\eta^2}\right)^2=0,\end{aligned} \quad (14)$$

$$\frac{\partial^2\phi(\eta)}{\partial\eta^2}+\frac{1}{2}Scf(\eta)\frac{\partial\phi(\eta)}{\partial\eta}+Sc\lambda\phi(\eta)=0. \quad (15)$$

And the boundary conditions, after applying the similarity variables (14) becomes

International Journal of Advances in Engineering and Management (IJAEM)
Volume 4, Issue 12 Dec. 2022, pp: 778-790 www.ijaem.net ISSN: 2395-5252

$$f'(0) = L_0\big(1-\beta\theta(0)\big)\frac{\partial^2 f(0)}{\partial\eta^2}, f(0) = S,$$
$$\big(1+\beta\theta(0)\big)\frac{\partial\theta(0)}{\partial\eta} = Bi(\theta(0)-1), \quad (16)$$
$$\frac{\partial\phi(0)}{\partial\eta} + Du\frac{\partial\theta(0)}{\partial\eta} = 0$$
$$f'(\infty)\to 1, \theta(\infty)\to 0, \phi(\infty)\to 0,$$

Where $S = f(0) = -\frac{v_0}{\sqrt{U_\infty \nu_f}}$, $S > 0$ and so(i.e.$v_0 < 0$)$S < 0$ $(i.e. v_0 > 0)$correspond to suction and blowing, respectively, L_0 is the velocity slip parameter, and Du (Duffor number) is the passive control parameter, and Bi is the local convective heat exchange parameter.

These are the obtained emergent flow governing parameters:

$$\frac{\sigma_0\beta_0^2}{\rho_f} = Ha, \quad \frac{g\beta_t(x)(T_w-T_\infty)}{U_\infty c\rho_f} = Grt,$$
$$\frac{g\beta_c(x)(C_w-C_\infty)}{U_\infty c\rho_f} = Grc, \frac{a}{c} = A, \frac{b_1(T_w-T_\infty)}{a} = \beta,$$
$$\frac{k_f}{\mu_f c_p} = \frac{1}{Pr}, \frac{Q}{c\rho_f c_p} = \delta, \frac{a^2x^2}{c_p(T_w-T_\infty)} = Ec,$$
$$\frac{D}{\nu_f\rho_f} = \frac{1}{Sc}, \frac{\kappa r^2}{c\rho_f} = \lambda, \frac{(T_w-T_\infty)}{(C_w-C_\infty)}\frac{D_T}{T_\infty D_B} = Du,$$
$$-\frac{v_0}{\sqrt{U_\infty\nu_f}} = S, L_1\mu_f\sqrt{\frac{a}{\nu_f}} = L_0, \frac{k_f}{h}\sqrt{\frac{a}{\nu_f}} = \frac{1}{Bi}$$

2.2 Flow Rate at the wall

The skin-friction parameter, plate surface temperature, Nusselt number, and Sherwood number are some other physical parameters of engineering significance in this situation that can be easily determined. To determine the total skin-friction, total heat, and total mass transfer rates for the local similarity example, integration across the entire plate is required. According to [31], these metrics, which describe the wall nano heat and mass transfer rates, are as follows:

$$c_{f_x} = \frac{\tau_w}{\rho_{nf}U_w^2}, \; Nu_x = \frac{xq_w}{k_{nf}(T_w - T_\infty)}, \; Sh_x = \frac{xq_m}{D_B(C_w - C_\infty)} \quad (17)$$

where τ_w, q_w and q_m respectively represents the heat and mass fluxes at the surface, the skin friction along the surface, and the heat flux from the surface, they are given as

$$\tau_w = \left[(\mu_T)\frac{\partial u}{\partial y}\right]_{y=0}, q_w = \left[-k_T\frac{\partial T}{\partial y}\right]_{y=0}, \quad (18)$$
$$q_m = \left[-D_B\frac{\partial C}{\partial y}\right]_{y=0}$$

When the similarity transformation is applied to (17) subject to (18), we get the result

$$\tau = (Re_x)c_{f_x} = \big(1-\beta\theta(\eta)\big)\frac{\partial^2 f(\eta)}{\partial\eta^2}\bigg|_{\eta=0}$$
$$Nu = \frac{Nu_x}{\sqrt{Re_x}} = -\big(1+\alpha\theta(\eta)\big)\frac{\partial\theta(\eta)}{\partial\eta}\bigg|_{\eta=0} \quad (19)$$
$$Sh = \frac{Sh_x}{\sqrt{Re_x}} = \frac{\partial\phi(\eta)}{\partial\eta}\bigg|_{\eta=0}$$

III NUMERICAL SOLUTION

The Homotopy analysis method (HAM) is a method of analysis that involves assembling a number of basis functions to symbolize the problem at hand. The fundamental operations are chosen to be, and. These are characterized as follows due to the exponential decrease of boundary layer fluxes at infinity: Liao [32, 33].

$$f(\eta) = a_{0,0} + \sum_{k=0}^{\infty}\sum_{n=0}^{\infty} a_{k,n}\eta^k e^{-n\eta},$$
$$g(\eta) = \sum_{k=0}^{\infty}\sum_{n=0}^{\infty} b_{k,n}\eta^k e^{-n\eta}, \quad (23)$$
$$\theta(\eta) = \sum_{k=0}^{\infty}\sum_{n=0}^{\infty} c_{k,n}\eta^k e^{-n\eta}$$

The basic function solution rule must be followed. We carefully choose the initial approximations using the boundary conditions as follows:

$$f(\eta) = 1 + \frac{1}{A+U_{slip}}(1-e^{-\eta}),$$
$$\theta(\eta) = -\frac{\beta_i}{N_3}(1-e^{-\eta}), \quad (24)$$
$$\phi(\eta) = e^{-\eta}$$

Next, which signify the auxiliary linear operators are chosen as follows:

$$L_f(f) = f''(\eta) - f(\eta),$$
$$L_\theta(\theta) = \theta''(\eta) - \theta(\eta), \quad (25)$$
$$L_\phi(\phi) = \phi''(\eta) - \phi(\eta)$$

The above equation (3) satisfies the following

$$L_f(c_1 + c_2 + c_3e^{\eta} + c_4e^{-\eta}) = 0,$$
$$L_\theta(c_5e^{\eta} + c_6e^{-\eta}) = 0, \quad (26)$$
$$L_\phi(c_7e^{\eta} + c_8e^{-\eta}) = 0$$

where the c_s are constants.

If the embedding and non-zero parameters are given as $0 \le p \le 1$, and (h_f, h_θ, h_ϕ)

International Journal of Advances in Engineering and Management (IJAEM)
Volume 4, Issue 12 Dec. 2022, pp: 778-790 www.ijaem.net ISSN: 2395-5252

respectively, then the deformation problems (of zeroth order) are:

$$(1-p)L_f[f(\eta,p)-f_0(\eta)] = phN_f[f,\theta,\phi],$$
$$(1-p)L_\theta[\theta(\eta,p)-\theta_0(\eta)] = phN_\theta[f,\theta,\phi], \quad (27)$$
$$(1-p)L_\phi[\phi(\eta,p)-\phi_0(\eta)] = phN_\phi[f,\theta,\phi].$$

Thus

$$N_f[f,\theta,\phi] = \frac{\partial}{\partial\eta}\left(\left(1-\beta\theta(\eta,p)\right)\frac{\partial^2 f(\eta,p)}{\partial\eta^2}\right) + \frac{1}{2}f(\eta)\frac{\partial^2 f(\eta,p)}{\partial\eta^2} + Ha\left(1-\frac{\partial f(\eta,p)}{\partial\eta}\right) + Grt\theta(\eta,p) + Grc\phi(\eta,p) + A^2 \quad (28)$$

$$N_\theta[f,\theta,\phi] = \frac{\partial}{\partial\eta}\left(\left(1+\alpha\theta(\eta,p)\right)\frac{\partial\theta(\eta,p)}{\partial\eta}\right) + \frac{1}{2}Prf(\eta,p)\frac{\partial\theta(\eta,p)}{\partial\eta} + Pr\delta\theta(\eta,p) + PrEc\left(\frac{\partial^2 f(\eta,p)}{\partial\eta^2}\right)^2 \quad (29)$$

$$N_\phi[f,\theta,\phi] = \frac{\partial^2\phi(\eta,p)}{\partial\eta^2} + Sc\lambda\phi(\eta,p) + \frac{1}{2}Scf(\eta,p)\frac{\partial\phi(\eta,p)}{\partial\eta} = 0. \quad (30)$$

with the boundary conditions

$$f'(0,p) = L_0\left(1-\beta\theta(\eta)\right)\frac{\partial^2 f(0,p)}{\partial\eta^2},$$
$$\left(1+\alpha\theta(0,p)\right)\frac{\partial\theta(0,p)}{\partial\eta} = Bi(\theta(0,p)-1), \quad (31)$$
$$f(0,p) = S, \frac{\partial\phi(0,p)}{\partial\eta} + Du\frac{\partial\theta(0,p)}{\partial\eta} = 0,$$
$$f'(\infty,p)\to 1, \theta(\infty,p)\to 0, \phi(\infty,p)\to 0,$$

For $p = 0, f(\eta,0) = f_0(\eta), \theta(\eta,0) = \theta_0(\eta)\ and\ \phi(\eta,0) = \phi_0(\eta)$ and for $p = 1, f(\eta,1) = f(\eta), \theta(\eta,1) = \theta(\eta)\ and\ \phi(\eta,1) = \phi(\eta)$

As p changes from 0 to 1, $f_0(\eta), \theta_0(\eta)\ and\ \phi_0(\eta)$ approach $f(\eta,p), \theta(\eta,p)\ and\ \phi(\eta,p)$ respectively.

The series in (23) converges at $p = 1$ when the auxiliary parameter is at the proper value.

The general answers to the non-homogeneous equations are

$$f_\infty(\eta) = f_m^*(\eta) + c_1^m + c_2^m + c_3^m e^\eta + c_4^m e^{-\eta},$$
$$\theta_\infty(\eta) = \theta_m^*(\eta) + c_5^m e^\eta + c_6^m e^{-\eta}, \quad (32)$$
$$\phi_\infty(\eta) = \phi_m^*(\eta) + c_7^m e^\eta + c_9^m e^{-\eta}$$

And then the equations are coded using numeric solver embedded in Maple 2021 software.

IV RESULTS AND DISCUSSION

In other to analyse and clarify the effect of flow governing parameters on the velocity, temperature and concentration fields, we choose our base line $A = 0, Bi = 0.05, Du = 0, Ec = 0, Grc = 0, Grt = 0, Ha = 0, Pr = 0.72, S = 0, Sc = 0.63, \alpha = 0, \beta = 0, \delta = 0, \lambda = 0, L_0 = 0$ as prescribe parameters The computations were done by a program which uses a symbolic and computational computer language MAPLE. A step size of $\Delta\eta = 0.001$ was selected to be satisfactory for a convergence criterion of 10^{-7} in nearly all cases. The value of η_∞ was found to each iteration loop by the assignment statement $\eta_\infty = \eta_\infty + \Delta\eta$. The maximum value of η_∞, to each group of parameters is determined when the values of unknown boundary conditions at $\eta = 0$ not change to successful loop with error less than 10^{-7}. The result thus obtained is discussed as follows.

4.1 Result Validation: The results obtain inthis report are validated by comparing with those obtained Aziz [34] and Makinde [33] and were found to be in excellent agreement as shown in Table 1

Table 1. Comparison with existing results for $M = Gr = \lambda = \alpha = Br = L_0 = S = Du = 0.0$ and for different convective surface boundary condition (Bi)

Bi	Aziz et.al [34]		Makinde [33]		Present Result	
	$\theta(0)$	$\theta'(0)$	$\theta(0)$	$\theta'(0)$	$\theta(0)$	$\theta'(0)$
0.05	0.1447	0.0428	0.14466	0.04276	0.144651	0.042767
0.10	0.2528	0.0747	0.25275	0.07472	0.252743	0.074726
0.20	0.4035	0.1193	0.40352	0.11929	0.403503	0.119299
0.40	0.5750	0.1700	0.57501	0.16999	0.574994	0.170002
0.60	0.6699	0.1981	0.66991	0.19805	0.669815	0.198111
0.80	0.7302	0.2159	0.73016	0.21586	0.730085	0.215932
1.00	0.7718	0.2282	0.77182	0.22817	0.771749	0.228251
5.00	0.9441	0.2791	0.94417	0.27913	0.944156	0.279221
10.00	0.9713	0.2871	0.97128	0.28714	0.971276	0.287239
20.00	0.9854	0.2913	0.98543	0.29132	0.985429	0.291422

International Journal of Advances in Engineering and Management (IJAEM)
Volume 4, Issue 12 Dec. 2022, pp: 778-790 www.ijaem.net ISSN: 2395-5252

4.2. Velocity distribution: The velocity distributions was depicted using Figures 2 to 5 where the variation of stretching velocity, Hartman number, thermal buoyancy and temperature dependent viscosity with were displayed. From Figure 2-3, an increase in stretching velocity, Hartman number and thermal buoyancy respectively are seen to increase velocity distributions. At about 2unit distance from the wall, increasing the stretching parameter by 0.1 unit brings about 15.5% increment in velocity, further increase by 0.1 units resulted into 8.6% increase in velocity and by increasing the stretching parameter to 0.3 unit which is equivalent of 50% increment, corresponding 6.6% increase in velocity was realized. Thus, continuous increments in stretching parameter leads to a free stream velocity. The effect of Hartman number is reversed for passive control flow as increment in Lorentz force decline the velocity boundary layer and bring the flow velocity to a free stream velocity faster than what could be experienced in active control flow. It could also be seen that those parameters bring about decrease in velocity boundary layer with occurrence of peak in Figure 4 due to higher thermal buoyancy. Velocity increases by 13.0%, 6.4% and 3.4% for each increase of thermal buoyancy parameter to 0.2, 0.3 and 0.4 values respectively. The analysis also indicates that as thermal buoyancy increases, the velocity boundary layer decrease. The temperature dependent viscosity is seen to enhance the velocity distribution as shown in Figure 5. From this Figure, it was discovered that increase in temperature dependent viscosity resulted in lowering the velocity boundary layer and increases the velocity distribution.

4.3. Energy distribution: We displayed the effect of suction parameter on the temperature distribution in as shown in Figure 6, from where we discovered that suction decline the temperature. This is as a result of energy being sucked away from the system leaving behind a lower energy content. In Figure 7 increase in heat absorption decline the temperature whereas, heat generation raises the energy content of the system. At each value of the heat generation/absorption parameter, the convective heat transfer is seen to play a major role in the temperature distribution. This determine the rate at which heat is transferred across the wall. Increasing the suction parameter from 0 to 2, followed by 0.4 and 0.8 brings about corresponding 14.9%, 9.3% and 13.9% increase in temperature respectively. Figure 7 shows that heat generation decline and heat absorption increases the temperature distribution respectively. The effect of both convective heat transfer Bi and Eckert number are shown in Figures 8 and 9 respectively. It was discovered that convective heat transfer reduces the temperature distribution. We also observed that at value of $Bi > 0$, the effect of further increments in Bi is less significant. While increase in Eckert number resulted in temperature enhancement. Increase Eckert number by 300% increases the temperature at the wall by 41.2% and further increase of Eckert number by 100% and 25% resulted in temperature increment by 32% and 28.5% as shown in Figure 9 respectively.

4.4. Concentration distribution: Concentration distributions wea analysed by the effect of mass buoyancy, convective heat transfer, chemical reactivity parameter and Dufort (Du) number as displayed in Figure 10-13 respectively. From these figures, increase in mass buoyancy as well as the flow passive control parameter Du brings about increase in concentration distribution as displayed in Figure 10 and Figure 13 respectively. While in Figure 11, temperature dependent viscousity parameter is seen to increase the chemical species concentration. In Figure 12, destructive chemical reaction ($\lambda < 0$) lowers the species concentrations whereas, generative chemical reaction corresponding to $\lambda > 0$ increases the species concentrations.

4.4. Concentration distribution: Concentration distributions wea analysed by the effect of mass buoyancy, convective heat transfer, chemical reactivity parameter and Dufort (Du) number as displayed in Figure 10-13 respectively. From these figures, increase in mass buoyancy as well as the flow passive control parameter Du brings about increase in concentration distribution as displayed in Figure 10 and Figure 13 respectively. While in Figure 11, temperature dependent viscousity parameter is seen to increase the chemical species concentration. In Figure 12, destructive chemical reaction ($\lambda < 0$) lowers the species concentrations whereas, generative chemical reaction corresponding to $\lambda > 0$ increases the species concentrations.

4.4 Wall Rate Transfer: Table 2 display the effect of the flow governing parameters on skin-Friction (τ), heat transfer at the wall (NU) and mass transfer rate at the wall. So also, the table shows the corresponding values of the initial conditions for momentum, energy and concentration equations. From the table, increase stretching parameter, Hartman number, thermal Grashof number, heat

International Journal of Advances in Engineering and Management (IJAEM)
Volume 4, Issue 12 Dec. 2022, pp: 778-790 www.ijaem.net ISSN: 2395-5252

generation parameter and Eckert number result in decrease in τ, Nu and Sh. The effect of other parameters was represented and self-explained in the table. In Table 3, the effect of temperature dependent viscousity and thermal conductivity, Convective heat transfer, slip velocity and suction parameters on was shown τ, Nu and Sh as well as the equivalent initial conditions on the flow field. The characteristics effect of the parameters is well explained by the table.

Table 2: Impact of flow parameters on transfer rate at the wall

	$f'(0)$	$f''(0)$	$\phi(0)$	$\theta(0)$	$\theta'(0)$	τ	Nu	Sh
A=0.0	0.14221	0.87324	-0.03398	0.46419	-0.03113	0.01279	0.04776	0.01245
A=0.1	0.14523	0.89463	-0.03332	0.47069	-0.03082	0.01267	0.04735	0.01233
A=0.2	0.15418	0.95972	-0.03134	0.49168	-0.02982	0.01227	0.04614	0.01193
A=0.3	0.16876	1.07154	-0.02810	0.53120	-0.02789	0.01149	0.04409	0.01116
Ha =0.0	0.10980	0.84636	-0.00910	0.87877	-0.00828	0.00333	0.01587	0.00331
Ha =0.4	0.14129	1.17615	-0.00012	0.99835	-0.00012	0.00005	0.00026	0.00005
Ha =0.8	0.16112	1.45690	0.00886	1.11764	0.00885	-0.00349	-0.02329	-0.00354
Ha =1.2	0.17369	1.75801	0.02088	1.26562	0.02137	-0.00823	-0.06733	-0.00855
Grt =0.0	0.09904	0.79250	-0.04892	0.93783	-0.04331	0.01792	0.08527	0.01732
Grt =0.2	0.13820	1.16480	0.01217	1.01698	0.01204	-0.00475	-0.02660	-0.00482
Grt =0.3	0.15840	1.40731	0.06765	1.09304	0.06921	-0.02499	-0.17172	-0.02769
Grt =0.4	0.18156	1.79572	0.17368	1.23647	0.18782	-0.04979	-0.55930	-0.07513
$Grc = -0.4$	0.17233	1.49702	0.04403	1.06101	0.04464	-0.01666	-0.11395	-0.01786
Grc =0.4	0.17639	1.55206	0.05751	1.07941	0.05872	-0.02135	-0.15385	-0.02349
Grc =0.8	0.17940	1.59320	0.06691	1.09245	0.06876	-0.02449	-0.18337	-0.02751
Grc =1.2	0.18346	1.64885	0.07914	1.10957	0.08199	-0.02836	-0.22393	-0.03280
$\lambda = -0.2$	0.17477	1.52814	0.03519	1.07050	0.05182	-0.01909	-0.09275	-0.02073
$\lambda = -0.1$	0.17484	1.53145	0.04031	1.07290	0.05375	-0.01973	-0.10653	-0.02150
λ =0.1	0.17517	1.53586	0.05388	1.07436	0.05487	-0.02010	-0.14278	-0.02195
λ =0.15	0.17531	1.53533	0.05765	1.07282	0.05358	-0.01967	-0.15262	-0.02143
$\delta = -0.6$	0.17167	1.10681	-0.27582	0.56125	-0.26380	0.13633	0.44715	0.10552
$\delta = -0.2$	0.17326	1.20504	-0.19367	0.70274	-0.18834	0.09243	0.35767	0.07533
δ =0.1	0.17488	1.39205	-0.04876	0.92967	-0.04876	0.02083	0.11187	0.01951
δ =0.2	0.17517	1.53354	0.05214	1.07224	0.05314	-0.01952	-0.13787	-0.02126
Ec =0.1	0.17351	1.17558	-0.22088	0.65506	-0.21465	0.10753	0.39098	0.08586
Ec =0.4	0.17458	1.28306	-0.13378	0.79914	-0.13210	0.06180	0.27095	0.05284
Ec =0.8	0.17517	1.53586	0.05388	1.07436	0.05487	-0.02010	-0.14278	-0.02195
Ec =1.0	0.17339	1.91078	0.29409	1.36592	0.30985	-0.05056	-1.06166	-0.12394
Du =0.2	0.13798	1.16261	0.00591	1.01650	0.01170	-0.00231	-0.01290	-0.00234
Du =0.4	0.13822	1.16737	0.01473	1.01997	0.01439	-0.00566	-0.03226	-0.00576
Du =0.8	0.13881	1.17373	0.03203	1.02174	0.01567	-0.01231	-0.07045	-0.01254
Du =1.4	0.13987	1.18505	0.06349	1.02468	0.01779	-0.02438	-0.14059	-0.02491

Table 3: Effect of variable viscousity, variable thermal conductivity, slips, suction and convective heat transfer condition on flow rate at the wall

International Journal of Advances in Engineering and Management (IJAEM)
Volume 4, Issue 12 Dec. 2022, pp: 778-790 www.ijaem.net ISSN: 2395-5252

	$f'(0)$	$f''(0)$	$\phi(0)$	$\theta(0)$	$\theta'(0)$	τ	Nu	Sh
$\alpha = -0.50$	0.17565	1.58637	0.12839	1.11604	0.13105	-0.04152	-0.35568	-0.05242
$\alpha = -0.30$	0.17517	1.53586	0.05388	1.07436	0.05487	-0.02010	-0.14278	-0.02195
$\alpha = -0.10$	0.17538	1.50307	0.02274	1.04145	0.02313	-0.00893	-0.05834	-0.00925
$\alpha = 0.00$	0.17560	1.48893	0.01265	1.02582	0.01291	-0.00506	-0.03197	-0.00516
$\beta = 0.40$	0.17517	1.53354	0.05214	1.07224	0.05314	-0.01952	-0.13787	-0.02126
$\beta = 0.10$	0.19654	1.08438	-0.04424	0.93784	-0.04325	0.01811	0.08923	0.01730
$\beta = -0.40$	0.21813	0.81071	-0.09750	0.86330	-0.09224	0.03965	0.16573	0.03689
$\beta = -0.80$	0.23092	0.69268	-0.11943	0.83343	-0.11107	0.04785	0.18838	0.04443
Bi =0.10	0.17092	1.75821	0.04482	1.28542	0.04638	-0.01704	-0.14612	-0.01855
Bi =0.50	0.17517	1.53586	0.05388	1.07436	0.05487	-0.02010	-0.14278	-0.02195
Bi =1.00	0.17578	1.50507	0.05733	1.04007	0.05824	-0.02125	-0.14707	-0.02329
Bi =7.50	0.17638	1.47537	0.05960	1.00564	0.06051	-0.02204	-0.14803	-0.02420
L_0 =0.05	0.04331	1.82465	0.25575	1.31322	0.25839	-0.05463	-0.86858	-0.10336
L_0 =0.10	0.09347	1.88674	0.20568	1.26145	0.21032	-0.05074	-0.69520	-0.08413
L_0 =0.20	0.17517	1.53586	0.05388	1.07436	0.05487	-0.02010	-0.14278	-0.02195
L_0 =0.40	0.30504	1.18479	-0.07232	0.89088	-0.07450	0.03243	0.14865	0.02980
S =0.00	0.13993	1.43312	0.27907	1.27978	0.22684	-0.06124	-0.79092	-0.09074
S =0.20	0.14793	1.35959	0.11824	1.14011	0.10626	-0.03636	-0.30153	-0.04250
S =0.40	0.15624	1.34011	0.03099	1.04275	0.03100	-0.01188	-0.07430	-0.01240
S =0.80	0.17397	1.35756	-0.05711	0.89810	-0.06978	0.03056	0.12673	0.02791

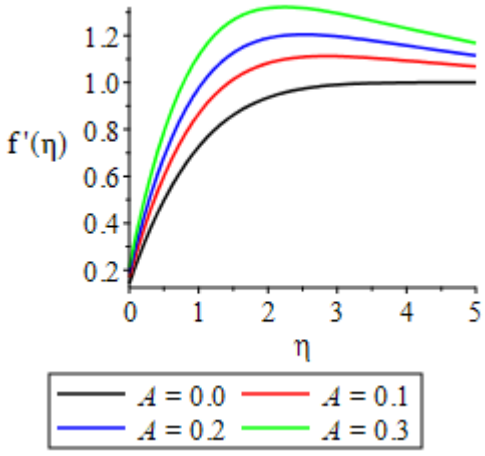

Figure 2: Velocity distribution for various stream velocity A

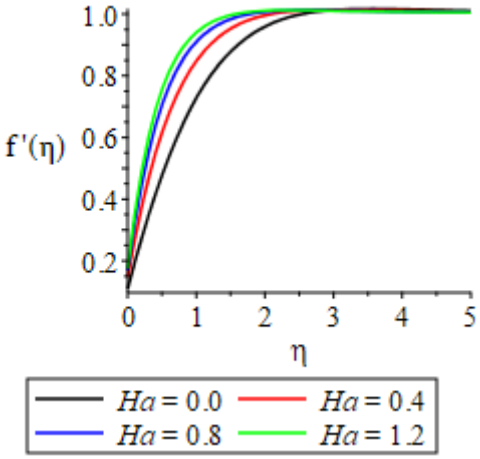

Figure 3: Variation of velocity with various values Hartman number

International Journal of Advances in Engineering and Management (IJAEM)
Volume 4, Issue 12 Dec. 2022, pp: 778-790 www.ijaem.net ISSN: 2395-5252

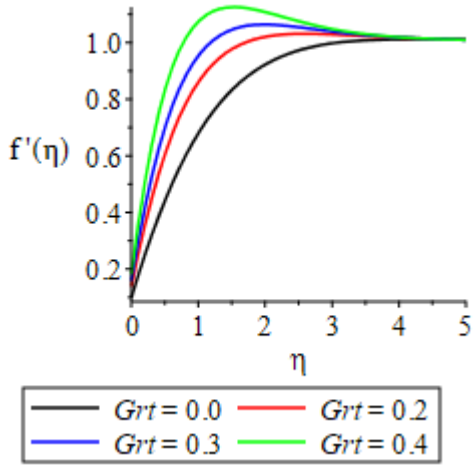

Figure 4: Effect of thermal Buoyancy on velocity

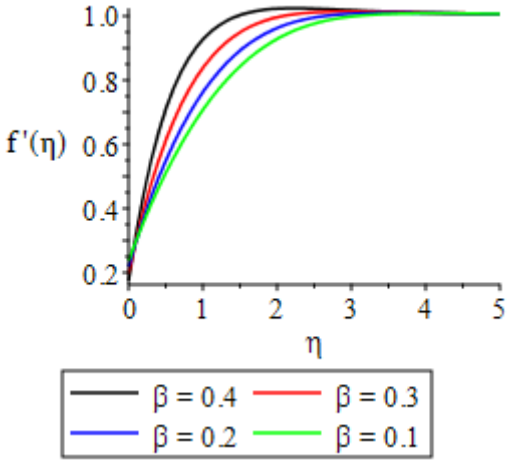

Figure 5: Effect of variable viscosity on velocity distribution

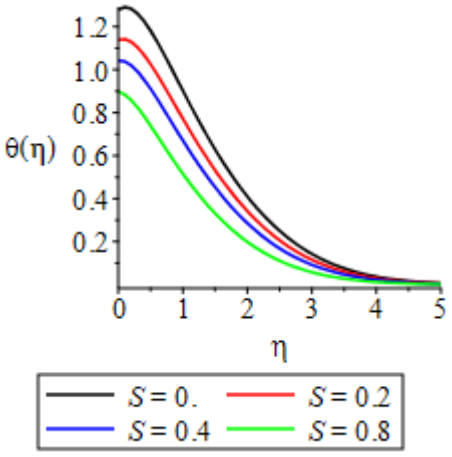

Figure 6: temperature profile for various suction parameter

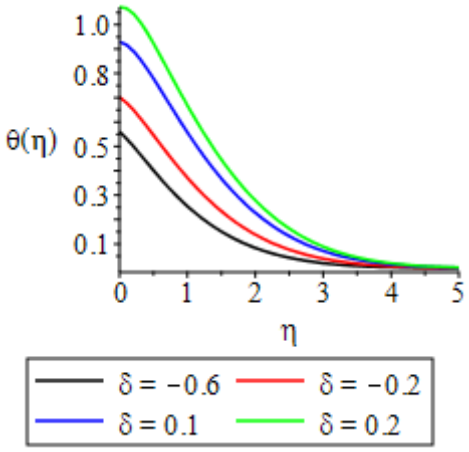

Figure 7: temperature profile for various heat generation/absorption

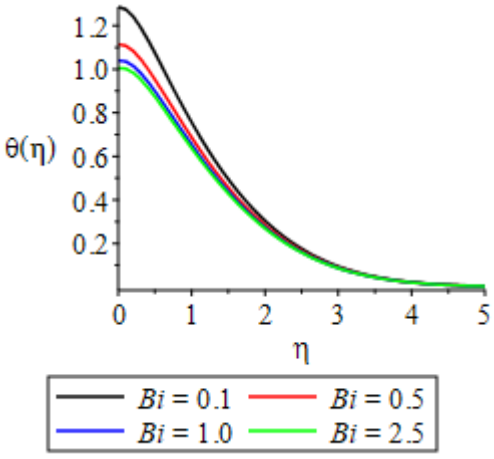

Figure 8: temperature profile for various convective heat transfer

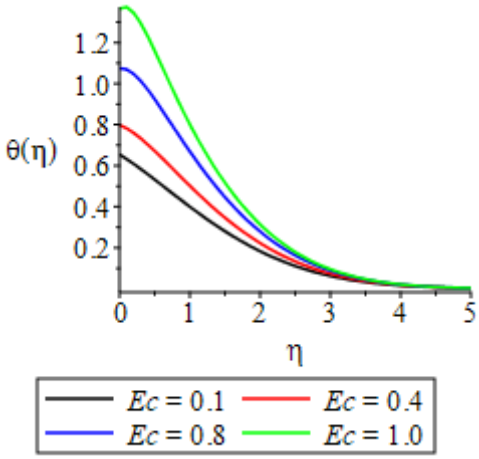

Figure 9: temperature profile for various values of Eckert number

International Journal of Advances in Engineering and Management (IJAEM)
Volume 4, Issue 12 Dec. 2022, pp: 778-790 www.ijaem.net ISSN: 2395-5252

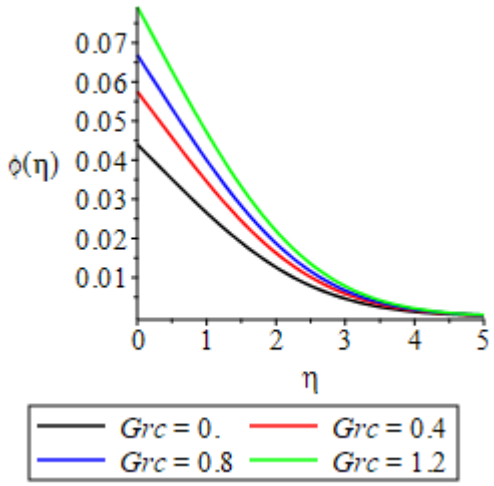

Figure 10: Chemical Species profile for various values of mass buoyancy

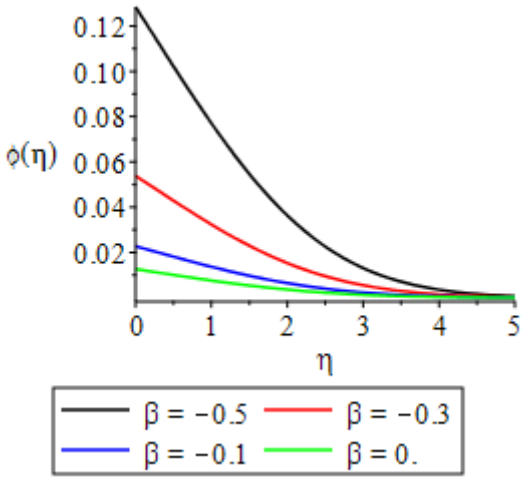

Figure 11: Chemical Species profile for various variable viscosity

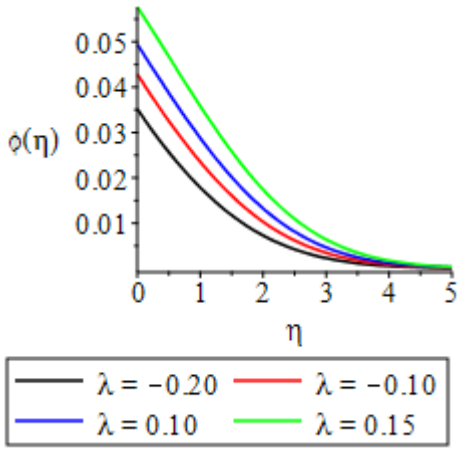

Figure 12: Chemical Species profile for various values of reactivity parameter

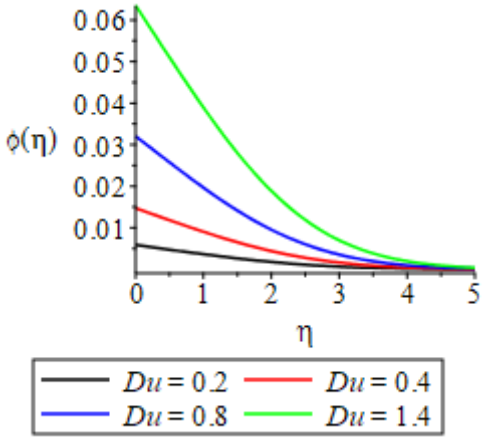

Figure 13: Chemical Species profile for various values of Dufort number

CONCLUSION:

From the Discussion above, the following conclusion were drawn

- increase in stretching velocity, Hartman number and thermal buoyancy respectively are seen to increase velocity distributions.
- continuous increments in stretching parameter leads to a free stream velocity.
- effect of Hartman number is reversed for passive control flow as increment in Lorentz force decline the velocity boundary layer
- temperature dependent viscosity enhance the velocity distribution
- that suction decline the temperature.
- increase in heat absorption decline the temperature
- that convective heat transfer reduces the temperature distribution.
- increase in Eckert number resulted in temperature enhancement.
- increase in mass buoyancy as well as the flow passive control parameter Du brings about increase in concentration
- temperature dependent viscousity parameter increase the chemical species concentration.
- increase stretching parameter, Hartman number, thermal Grashof number, heat generation parameter and Eckert number result in decrease in τ, Nu and Sh.

International Journal of Advances in Engineering and Management (IJAEM)
Volume 4, Issue 12 Dec. 2022, pp: 778-790 www.ijaem.net ISSN: 2395-5252

Nomenclature

x, y	flow axis
u, v	Velocity component along x and y-axis
T	Non-dimensional Temperature field
C	Non-dimensional Species concentration field
g	Acceleration due to gravity
B_0	Magnetic field of uniform strength
T_w	surface temperature
T_∞	ambient temperature
C_w	surface concentration
C_∞	ambient concentration
β_t	Volumetric coefficient of thermal expansion
β_c	Volumetric coefficient of mass expansion
k	thermal conductivity
c_p	specific heat capacity at constant pressure
D	Molecular diffusivity
U_∞	ambient velocity
Q	Heat source/sink parameter
G	reactivity parameter

Greek Symbol	
ρ	fluid density
σ	Electrical conductivity
ψ	stream function
Dimensionless group	
Bi	Convective heat transfer
θ	dimensionless temperature
ϕ	dimensionless concentration
Grt	Grashof number for mass transfer
Grc	buoyancy ratio
λ	Chemical reaction parameter
α	heat generation parameter
M	Magnetic parameter
Pr	Prandtl number
Sc	Schmidt number
Nu	Nusselt number
Sh	Sherwood number
Subscript	
∞	ambient condition
w	wall condition

AUTHOUR CONTRIBUTION
All authours contributed equally

CONFLICT OF INTEREST: The authours declare that there is no conflict of interest.

ACKNOWLEDGEMENTS: The authors would like to appreciate and thank Covenant University management for providing the enabling environment, research facilities. Also, we thank the anonymous referees for their useful suggestions that leads to improvement of the result.

REFERENCE

[1]. Nguyen, C. T., (2012), "Fundamentals of Mass Transport in microscale,"., second edition, http://doi.org/1016/B978 - 1 - 4377-3520-8.00002 – 4.

[2]. Nguyen CT, Desgranges F, Roy G, Galanis N, Mare T, Boucher S and Angue Minsta H, (2007), "Temperature and particle-size dependent viscosity data for water based nanofluids – hystresis phenomenon". Int. J. Heat Fluid Flow 28, 1492–1506 (2007).

[3]. Angue M, Roy HG, Nguyen CT and Doucet D (2009) "New temperature and conductivity data for water-based nanofluids". Int. J.Therm. Sci. 48 (2), 363–371,

[4]. Abu-Nada, E. (2009) "Effects of variable viscosity and thermal conductivity of water nanofluid" Int. J. Heat Fluid Flow (2009), https://doi.org/10.1016/j.ijheatfluidflow.2009.02.003.

[5]. Uddin, M. J., Khan, W. A., & Ismail, A. I. (2012). MHD Free Convective Boundary Layer Flow of a Nanofluid past a Flat Vertical Plate with Newtonian Heating Boundary Condition. PLoS ONE, 7(11), 49499. https://doi.org/10.1371/journal.pone.0049499

[6]. Animasaun I. L. and Sandeep, N., (2016) "Buoyancy induced model for the flow of 36 nm alumina-water nanofluid along upper horizontal surface of a paraboloid of revolution with variable thermal conductivity and viscosity" Power Technology **301**, 858 - 867. https://doi.org/10.1016/j.powtec.2016.07.023.

[7]. Kelvin O. Ogboru1, Azeez. A. Waheed2, Akindele. M. Okedoye: MHD Active Control Flow of Nanoparticles with Buoyancy and Variable Viscosity and Thermal Conductivity. Journal of Scientific and Engineering Research, 2022, 9(3):110-120

[8]. A. M. Okedoye*1, J. S. Damisa2, B. B. Malemi3 and Kelvin O. Ogboru. "Buoyancy Effect on MHD Nanofluid flow over a Porous Medium In the presence of Dufour and Ohmic Heating." IOSR Journal of Mathematics (IOSR-JM), 18(2), (2022): pp. 26-39. https://doi.org/10.9790/5728-1802022639.

[9]. Samad, M. A., & Mansur-Rahman, M. (1970). Thermal Radiation Interaction with Unsteady MHD Flow Past a Vertical Porous Plate Immersed in a Porous Medium. Journal of Naval Architecture and Marine Engineering, 3(1), 7–14.
[10]. Hossain, Md.Anwar, & Munir, M. S. (2000). Mixed convection flow from a vertical flat plate with temperature dependent viscosity. International Journal of Thermal Sciences, 39(2), 173–183.
[11]. Fang, T. (2004). Influences of fluid property variation on the boundary layers of a stretching surface. Acta Mechanica, 171(1–2).
[12]. Mahmoud, M. A. A. (2007). Variable viscosity Effects on hydromagnetic boundary layer flow along a continuously moving vertical plate in the presence of radiation. Applied Mathematical Sciences, 1(17), 799–814.
[13]. Hossain, M.Anwar, Khanafer, K., & Vafai, K. (2001). The effect of radiation on free convection flow of fluid with variable viscosity from a porous vertical plate. International Journal of Thermal Sciences, 40(2), 115–124.
[14]. Poornima, T., & N.B., R. (2013). Radiation effects on MHD free convective boundary layer flow of nanofluids over a nonlinear stretching sheet. Advances in Applied Science Research, 4(2), 190–202.
[15]. Kandasamy, R., Muhaimin, I., & Mohamad, R. (2013). Thermophoresis and Brownian motion effects on MHD boundary-layer flow of a nanofluid in the presence of thermal stratification due to solar radiation. International Journal of Mechanical Sciences, 70, 146–154.
[16]. Motsumi, T. G., & Makinde, O. D. (2012). Effects of thermal radiation and viscous dissipation on boundary layer flow of nanofluids over a permeable moving flat plate. Physica Scripta, 86(4), 045003.
[17]. Bataller, R. C. (2008). Radiation effects for the Blasius and Sakiadis flows with a convective surface boundary condition. Applied Mathematics and Computation - Elsevier-, 206(2), 832–840.
[18]. Makinde, O. D., & Aziz, A. (2010). Second law analysis for a variable viscosity plane Poiseuille flow with asymmetric convective cooling. Computers and Mathematics with Applications, 60, 3012–3019.
[19]. Makinde, O. D., &Bég, O. A. (2010). On inherent irreversibility in a reactive hydromagnetic channel flow. Journal of Thermal Science, 19(1), 72–79.
[20]. Narusawa, U. (2001). The second-law analysis of mixed convection in rectangular ducts. Heat and Mass Transfer 2001 37:2, 37(2), 197–203.
[21]. Bejan, A. (1982). Second-Law Analysis in Heat Transfer and Thermal Design. 15, 1–58. https://doi.org/10.1016/S0065-2717(08)70172-2.
[22]. Bejan, A. (1998). Entropy generation minimization: The new thermodynamics of finite-size devices and finite-time processes. Journal of Applied Physics, 79(3), 1191.
[23]. Okedoye A. M., Damisa J. S., Malemi B. B. and Kelvin O. Ogboru. Buoyancy Effect on MHD Nanofluid flow over a Porous Medium In the presence of Dufour and Ohmic Heating. IOSR Journal of Mathematics (IOSR-JM). 18(2),2022a Ser. II, PP 26-39. DOI: http://dx.doi.org//10.9790/5728-1802022639
[24]. Okedoye A. M. and Salawu S. O.,Unsteady oscillatory MHD boundary layer flow past a moving plate with mass transfer and binary chemical reaction. SN Applied Sciences 1,2019,1586 https://doi.org/10.1007/s42452-019-1463-7.
[25]. Akindele M. Okedoye and Sulyman O. Salawu (2019): Effect of Nonlinear Radiative Heat and Mass Transfer on MHD Flow over a Stretching Surface with Variable Conductivity and Viscosity. Journal of the Serbian Society for Computational Mechanics / Vol. 13 / No. 2, 2019 / pp 86-103 https://doi:10.24874/jsscm.2019.13.02.07.
[26]. A.M. Okedoye and S.O. Salawu (2020): transient heat and mass transfer of hydromagnetic effects on the flow past a porous medium with movable vertical permeablesheet. Int. J. of Applied Mechanics and Engineering, 2020, vol.25, No.4, pp.175-190. https://doi:10.2478/ijame-2020-0057 .
[27]. Hafiz Abdul Wahab, Hussan Zeb, Saira Bhatti, Muhammad Gulistan, Seifedine Kadry and Yunyoung Nam: Numerical Study for the Effects of Temperature Dependent Viscosity Flow of Non-Newtonian Fluid with Double Stratification.Appl. Sci. **2020**, 10, 708; http://dx.doi.org/10.3390/app10020708
[28]. N.A. Halim, S. Sivasankaran, N.F.M. Noor. Active and passive controls of the Williamson stagnation nanofluid flow over a

stretching/shrinking surface Neural Comput Appl (2016), https://doi.org/10.1007/s00521-016-2380-y

[29]. N.A. Halim, R.U. Haq, N.F.M. Noor Active and passive controls of nanoparticles in Maxwell stagnation point flow over a slipped stretched surface Meccanica, 52 (2017), pp. 1527-1539

[30]. T. Muhammad, A. Alsaedi, S.A. Shehzad, T. Hayat A revised model for Darcy-Forchheimer flow of Maxwell nanofluid subject to convective boundary condition. Chin J Phys, 55 (2017), pp. 963-76

[31]. O. D. Makinde (2010): Similarity solution of hydromagnetic heat and mass transfer over a vertical plate with a convective surface boundary condition. International Journal of the Physical Sciences Vol. 5(6), pp. 700-710, June 2010.

[32]. Liao Sj. The proposed homotopy analysis technique for the solution of non-linear problems (Ph.D. thesis), Shanghai Jiao Tong university; 1992.

[33]. Liao Sj. Beyond perturbation: introduction to homotopy analysis method. Boca Raton: Chapman & Hall/CRC Press; 2003.

[34]. Aziz A, Siddique J.I. Aziz T (2014) Steady Boundary Layer Slip Flow along with Heat and Mass Transfer over a Flat Porous Plate Embedded in a Porous Medium. PLoS ONE 9(12): http://dx.doi:10.1371/journal.pone.0114544.